JOURNAL OF AGRICULTURAL AND FOOD CHEMISTRY

Article

pubs.acs.org/JAFC

Iodine Bonding Stabilizes Iodomethane in MIDAS Pesticide. Theoretical Study of Intermolecular Interactions between Iodomethane and Chloropicrin

Rainer Glaser* and Kaitlan Prugger

Department of Chemistry, University of Missouri, Columbia, Missouri 65211, United States

Supporting Information

ABSTRACT: The results are reported of a theoretical study of iodomethane (H_3C-I, **1**) and chloropicrin (Cl_3C-NO_2, **2**), of the heterodimers **3**−**6** formed by aggregation of **1** and **2**, and of their addition products **7** and **8** and their possible fragmentation reactions to **9**−**18**. Mixtures of iodomethane and chloropicrin are not expected to show chemistry resulting from their reactions with each other. The structures and stabilities are discussed of the iodine-bonded molecular aggregates (IBMA) **3** and **4** and of the hydrogen- and iodine-bonded molecular aggregates (IHBMA) **5** and **6**. The mixed aggregates **3**−**5** are bound on the free enthalpy surface relative to the homodimers of **1** and **2**, and the IBMA structures **3** and **4** are most stable. This result suggests that the mixture of chloropicrin and iodomethane in the pesticide Midas is a good choice to reduce the volatility of iodomethane because of thermodynamically stabilizing iodine bonding.

KEYWORDS: *intermolecular bonding, halogen bonding, methyl iodide, chloropicrin, pesticide, soil fumigant, UHF instability*

INTRODUCTION

By the end of 2004 the U.S. Environmental Protection Agency (EPA) completed its phase-out of methyl bromide[1] as a pesticide because of the fumigant's contribution to atmospheric ozone depletion.[2] A number of alternatives for methyl bromide have been suggested for various uses,[3] and, in October 2007, its homologue methyl iodide (CH_3I, MeI, iodomethane) was approved for use a plant pesticide.[4] Even though the application of soil fumigants is highly regulated to minimize adverse health effects on agricultural works and the public,[5] the approval of methyl iodide has generated considerable controversy[6,7] because of its toxicology[8] and especially its carcinogenicity.[9]

Methyl iodide and other alkyl iodides are produced naturally by microorganisms in the surface layers of the oceans[10−14] with an estimated[15] global CH_3I emission into the atmosphere of 0.1−0.6 Tg I yr^{-1} (1 Tg = 10^{12} g). The relatively long atmospheric lifetime of methyl iodide allows for long distance transport[16] and an atmospheric concentration below 1 pptv depending on location and season.[15] Field volatility studies[17] showed that CH_3I concentrations would reach about 1 ppmv on the field shortly after the application and drop off quickly with distance from the field and over time. Fumigant volatilization studies showed that 20−80% of methyl iodide can be emitted into the atmosphere after its field application,[18,19] and, hence, approaches have been explored to minimize air pollution from soil fumigation and increase pesticide efficiency.[20−22]

MeBr and MeI are structurally and functionally similar. The boiling points of MeBr and MeI are 3.3 °C (37.9 °F) and 42.5 °C (108.5 °F), respectively, and Henry's law constants H(MeI) = 0.21 and H(MeBr) = 0.24 are similar, and both are much higher compared to other fumigants.[23] As with MeBr, MeI has a high propensity to partition into the gas phase, and this is a major reason for its application in mixtures with other, usually less volatile pesticides.[24−26] These other pesticides contain chlorinated pyridine moieties, for example, such as trifluoromethyl-2,3-dichloropyridine or (trifluoromethyl)pyridine-3-carbonitrile. Most commonly, however, MeI is applied as MIDAS,[27] a mixture of the pesticides methyl iodide and chloropicrin[20,28] (Cl_3C-NO_2, trichloronitromethane, TCNM) either in equal amounts or in various other mixing ratios. The boiling point of chloropicrin is 112 °C (233 °F). The application of liquid pesticides leads to soil wetting, mixing with water, and evaporation. Fumigation seeks to suffocate pests by creating a gaseous layer of pesticide gas above and within the soil, and the efficacy of fumigation therefore is related to the pesticide's volatility. The fumigant needs to be volatile enough to allow the applied liquid to evaporate to form gaseous pesticide. For best fumigant efficiency, the fumigant gas layer should persist for some time and the volatility of the applied liquid should be such that it delivers a sufficient gaseous fumigant concentration over time rather than a very high concentration for a short time.

We are interested in learning about the physical and chemical effects of the application of mixtures of chloropicrin and methyl iodide. Specifically, it is our hypothesis that methyl iodide is stabilized in liquid MIDAS by iodine bonding between iodomethane and chloropicrin. The term "halogen bonding" has been coined to refer to the attractive intermolecular interaction between organohalides R−X (primarily Br, I) and highly electronegative heteroatoms (primarily O, N), and iodine bonding is particularly effective.[29−31] With a view to the known formation of pyridinium iodides on treatment of

Received: September 19, 2011
Revised: January 18, 2012
Accepted: January 23, 2012
Published: February 8, 2012

pyridine and amine derivatives with MeI,[24,25,32−34] we examined whether methyl iodide might methylate or even add to chloropicrin and thereby cause synergistic effects as a result of the pesticide combination.[35]

Here we report the results of a higher level ab initio study of the structures and stabilities of aggregates formed between CH_3I, **1**, and chloropicrin, **2**, and of some of their addition products (Figure 1). We have determined the iodine-bonded molecular aggregates (IBMA) **3** and **4** and the hydrogen-bonded molecular aggregates (HBMA) **5** and **6**. The methylation of chloropicrin at one of the nitro-O atoms might result in addition products **7** and **8**, and, if accessible, **7** and **8** might serve as reactive intermediates with a number of possible reaction channels for fragmentation to **9**−**18**. However, the analysis of the thermochemistry of these fragmentation reactions and of their kinetic feasibilities shows that the thermal methylation of chloropicrin by methyl iodide does not occur to any significant extent. The isomerizations between aggregates **3**−**6** are fast, their equilibration is under thermodynamic control, and aggregates **3**−**5** are bound with respect to the homodimers of **1** and **2**. Chloropicrin and iodomethane form iodine-bonded aggregates, and for this reason chloropicrin is a good choice for the stabilization of iodomethane in MIDAS to minimize air pollution from soil fumigation.

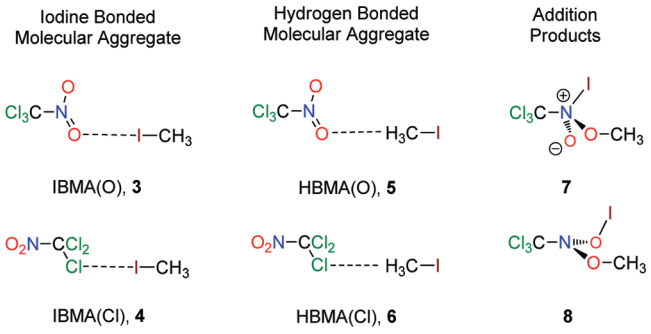

Figure 1. Types of aggregation between chloropicrin and methyl iodide.

THEORETICAL AND COMPUTATIONAL METHODS

Potential Energy Surface Analysis. To correctly assess intermolecular interactions requires correlated electronic structure methods that account for dispersion; hence, second-order Møller−Plesset perturbation theory (MP2) was employed for the potential energy surface analysis and more reliable energies were computed using quadratic configuration interaction theory including all single

Table 1. Total Energies and Thermochemical Data[a]

mol	E(MP2)	VZPE	TE	S	ν_1	ν_2	μ	E(QCI)
1	−6957.262929	23.73	25.70	60.56	549	948	2.13	−6957.252884
o-(**1**)$_2$	−13914.528074	47.75	53.17	110.32	10	21	3.68	−13914.507387
c-(**1**)$_2$	−13914.529556	47.93	53.23	106.89	13	19	0.00	−13914.508852
2a	−1621.390471	13.73	18.09	87.38	23	211	2.54	−1621.409473
2b	−1621.390311	13.69	17.50	81.08	−24	200	2.55	−1621.409334
c-(**2**)$_2$	−3242.786597	27.82	37.99	145.51	8	18	2.04	−3242.823495
3	−8578.657109	37.66	45.56	134.48	6	8	1.00	−8578.665282
			45.26	131.33	HR			
4	−8578.655288	37.60	45.56	138.10	3	12	4.70	−8578.666149
			45.26	133.59	HR			
5	−8578.659750	38.01	45.67	125.67	8	19	2.21	−8578.667680
6	−8578.655543	37.74	45.56	130.70	7	15	2.86	−8578.663806
7	−8578.626738	39.28	45.98	105.64	70	103	2.71	−8578.627562
8	−8578.623479	39.32	46.16	109.18	36	69	3.65	−8578.634140
TS(**7**,**8**)	−8578.582839	38.79	45.15	104.25	−51	61	7.21	−8578.608132
MRTS(**7**)	−8578.595994	38.51	44.95	103.49	−188	69	4.82	−8578.340517
MRTS(**8**)	−8578.599081	38.96	45.33	105.15	−158	40	5.15	−8578.610811
9	−8334.320121	5.64	9.36	83.33	182	182	0.58	−8334.323932
10a	−244.319937	30.79	33.73	68.47	107	233	2.93	−244.340517
10b	−244.323923	31.18	33.86	66.38	226	370	2.15	−244.343872
11	−1456.581623	30.91	34.46	77.61	256	256	2.06	−1456.630463
12	−7122.080504	7.15	9.72	71.98	204	298	2.48	−7122.040534
13a	−7122.066367	5.41	8.33	73.41	153	210	1.94	−7122.041376
13b	−7122.074941	5.93	8.57	71.84	195	387	1.81	−7122.049901
14	−1531.594977	33.50	37.84	84.44	82	211	2.44	−1531.644468
15	−7047.086056	3.69	5.96	67.69	220	471	2.54	−7047.053986
16	−7047.060719	3.88	6.29	68.88	167	327	5.90	−7047.039933
17	−1546.372660	9.71	13.71	82.52	76	222	0.84	−1546.408360
18	−7032.250398	26.62	29.14	69.25	247	296	1.75	−7032.241457
TS(**5**,**7**)	−8578.546300	37.28	44.12	109.41	−858	31	5.60	−8578.546780
TS(**5**,**8**)	−8578.550777	36.90	43.68	108.63	−521	26	5.34	−8578.541782

[a]All data based on RMP2(full)/6-31G* structures. E(QCI) values computed at the UQCISD/6-31G* level. Total energies (E) in atomic units, vibrational zero-point energies (VZPE) and thermal energies (TE) in kcal/mol, entropies (S) in cal/(mol·K), frequencies (ν_i) in cm^{-1}, and dipole moment (μ) in Debye

dx.doi.org/10.1021/jf2037906 | J. Agric. Food Chem. 2012, 60, 1776−1787

Table 2. Relative, Reaction, and Activation Energies[a]

rel or act. energy	ΔE	ΔH_0	ΔH_{298}	ΔG_{298}	$\Delta E'$	$\Delta G'$
E_{act}, **2b** vs **2a**	0.10	0.06	−0.49	1.39	0.09	1.38
2 **1** → c-(**1**)$_2$	−2.32	−1.86	−0.48	3.76	−1.94	4.14
2 **1** → o-(**1**)$_2$	−1.39	−1.11	0.39	3.61	−1.02	3.98
2 **2a** → c-(**2a**)$_2$	−3.55	−3.19	−1.75	6.98	−2.85	7.68
1 + **2a** → **3**, IBMA(O)	−2.33	−2.13	−0.56	3.45	−1.84	3.94
with hindered rotor			−0.86	4.10		4.59
1 + **2a** → **4**, IBMA(Cl)	−1.19	−1.05	0.59	3.52	−2.38	2.33
with hindered rotor			0.29	4.10		2.91
1 + **2a** → **5**, IHBMA(O)	−3.98	−3.44	−2.10	4.54	−3.34	5.18
1 + **2a** → **6**, IHBMA(Cl)	−1.34	−1.07	0.43	5.57	−0.91	6.00
c-(**1**)$_2$ + c-(**2a**)$_2$ → 2 **3**	0.61	0.40	0.55	−1.92	0.56	−1.97
with hindered rotor			0.26	−1.27		−1.32
c-(**1**)$_2$ + c-(**2a**)$_2$ → 2 **4**	1.75	1.47	1.70	−1.85	0.02	−3.58
with hindered rotor			1.40	−0.80		−2.53
c-(**1**)$_2$ + c-(**2a**)$_2$ → 2 **5**	−1.05	−0.92	−0.99	−0.83	−0.95	−0.73
c-(**1**)$_2$ + c-(**2a**)$_2$ → 2 **6**	1.59	1.46	1.54	0.20	1.49	0.10
E_{rel}(**8** vs **7**)	2.05	2.09	2.23	1.17	−4.13	−5.01
E_{act}(**7** → MRTS(**7**))	19.29	18.53	18.26	18.90	23.93	23.54
E_{act}(**8** → MRTS(**8**))	15.31	14.95	14.48	15.68	14.64	15.01
1 + **2a** → **7**	16.73	18.55	18.92	31.54	21.83	36.64
1 + **2a** → **8**	18.78	20.63	21.15	32.71	17.71	31.64
c-(**1**)$_2$ + c-(**2a**)$_2$ → 2 **7**	19.66	21.07	20.04	26.17	24.23	30.74
c-(**1**)$_2$ + c-(**2a**)$_2$ → 2 **8**	21.71	23.16	22.26	27.34	20.10	25.73
E_{rel}, **10a** vs **10b**	2.50	2.10	2.37	1.74	2.11	1.35
E_{rel}, **13a** vs **13b**	5.38	4.86	5.14	4.67	5.35	4.64
E_{rel}, **13b** vs **12**	3.49	2.28	2.34	2.38	−5.88	−6.99
E_{rel}, **16** vs **15**	15.90	16.09	16.23	15.88	8.82	8.80
A: **1** + **2a** → **9** + **10b**	5.87	5.24	5.31	4.78	−3.42	−4.51
B: **1** + **2a** → **11** + **12**	−5.48	−4.88	−5.09	−5.58	−5.42	−5.52
C: **1** + **2a** → **11** + **13**	3.39	2.26	2.39	1.47	−11.30	−13.22
D: **1** + **2a** → **14** + **15**	−17.34	−17.61	−17.33	−18.58	−22.65	−23.89
E: **1** + **2a** → **17** + **18**	19.04	17.90	18.10	16.96	7.87	5.79
E_{act}(**7** → TS(**7**,**8**))	27.55	27.06	26.71	27.13	12.19	11.77
E_{act}(**8** → TS(**7**,**8**))	25.50	24.97	24.49	25.96	16.32	16.78
E_{act}(**5** → TS(**5**,**8**))	66.72	65.96	64.85	72.56	76.57	82.41
E_{act}(**8** → TS(**5**,**8**))	45.62	43.20	43.14	43.31	57.96	55.65
E_{act}(**5** → TS(**5**,**7**))	71.19	70.46	69.64	74.49	75.87	79.17
E_{act}(**7** → TS(**5**,**7**))	50.48	48.48	48.61	47.49	50.69	47.70

[a]All data in kcal/mol. Energies (ΔE), enthalpies (ΔH_0, ΔH_{298}), and free enthalpies (ΔG_{298}) computed at MP2(full)/6-31G* level. Energies ($\Delta E'$) computed at UQCISD(full)/6-31G*//MP2(full)/6-31G* level and free enthalpies $\Delta G' = \Delta E' + (\Delta G_{298} - \Delta E)$.

and double excitations (QCISD).[36,37] All electrons were included in the active space, i.e., MP2(full) and QCISD(full). The standard 6-31G* basis set[38] was employed for H, C, N, O, and Cl atoms, iodine was described with a [10.9.5] contraction of a (15.12.7) basis set,[39] and in the following we refer to the resulting basis set simply as 6-31G* for brevity. Stationary structures of minima and transition state structures were optimized[40] and harmonic vibrational frequencies were computed at the RMP2(full)/6-31G* level, and results are listed in Table 1. Cartesian coordinates of all stationary structures are provided as Supporting Information. Relative, reaction, and activation energies are reported in Table 2 and include energies (ΔE), enthalpies ($\Delta H_0 = \Delta E + \Delta$VZPE, $\Delta H_{298} = \Delta E + \Delta$TE), and free enthalpies ($\Delta G_{298} = \Delta H_{298} - T{\cdot}\Delta S$) computed at MP2(full)/6-31G* level. In a few pertinent cases, the thermochemical analysis was refined by explicit treatment of internal hindered rotors.[41]

UHF Instabilities and UQCISD Computations. The restricted Hartree−Fock (RHF) wave functions were tested for possible UHF instabilities,[42,43] that is, it was examined whether the use of an unrestricted Hartree−Fock (UHF) wave function would lower the energy. UHF instabilities may occur for several reasons. Nitro compounds are isoelectronic with ozone, and the UHF instability of ozone is a well-known, classic case.[44] The UHF instability occurs because the spin-coupling of the electrons in one of the π-type MOs is weak and singlet biradical character becomes important. Similar phenomena have recently been reported for conjugated macrocycles[45] and for fullerenes and nanotubes.[46] Indeed, we found that chloropicrin does exhibit a UHF instability. With the UHF instability of **2**, one would expect UHF instabilities to occur in the homodimers of **2** and in its aggregates **3**−**6** formed with **1**, and these expectations are met with the exception of **4**. The restricted wave function of mixed aggregate **4** is stable. UHF instabilities also are to be expected in high-energy products formed by addition reactions which require the cleavage of σ-bonds and in the associated transition state structures. Indeed, stability tests for **7**, **8**, TS(**7**,**8**), TS(**5**,**7**) and TS(**5**,**8**) revealed UHF instabilities in all cases. The potential fragmentation reactions of **7** and **8** involve the products trichloroiodomethane (**9**, Cl_3C-I), methyl nitrite (**10**, H_3CO-NO), 1,1,1-trichloroethane (**11**, Cl_3C-CH_3), nitryl iodide (**12**, $I-NO_2$), nitrosyl hypoiodite (**13**, IONO), trichloromethyl methyl ether (**14**, $Cl_3C-O-CH_3$), nitrosyl iodide (**15**, I−N═O), isonitrosyl iodide (**16**, I−ON), trichloronitrosomethane (**17**, $Cl_3C-N{=}O$), and the methyl ester of hypoiodous acid (**18**, $IO-CH_3$). Several of the fragmentation products **9**−**18** also show UHF instabilities, and these

dx.doi.org/10.1021/jf2037906 | J. Agric. Food Chem. 2012, 60, 1776−1787

include the nitrites **10** and **13**, the nitro compound **12**, and the nitroso compounds **15**−**17**. The restricted wave functions of **9**, **11**, **14**, and **18** are stable.

Higher levels of electron correlation are required to compute reliable energies for significantly spin-polarized electronic systems; therefore, we determined energies at the UQCISD(full)/6-31G*//RMP2(full)/6-31G* level, and these results are included in Table 1 in the E(QCI) column. In Table 2 are provided the relative and reaction energies $\Delta E'$ computed at the UQCISD(full)/6-31G*//RMP2(full)/6-31G* level, and the free enthalpies $\Delta G' = \Delta E' + (\Delta G_{298} - \Delta E)$ include the thermochemical corrections computed at the level of optimization.

Electronic Structure and Molecular Properties. Electronic structures were characterized by population analysis,[47,48] by inspection of the molecular electrostatic potentials (ESP),[49] and by analyses of spin density distributions.[50]

Hardware and Sofware. Computations were performed with the quantum-mechanical software *Gaussian 09*[51] on the SGI Altix system (BX2 NUMA architecture machine with 64 1.5 GHz Intel Itanium2 processors and 128 GB of shared memory) of the Research Supporting Computing facility at the University of Missouri.

RESULTS AND DISCUSSION

Molecular Structures of Iodomethane and Chloropicrin. Molecular models of **1**, **2**, and their homodimers are shown in Figure 2. The computed structure of iodomethane **1**

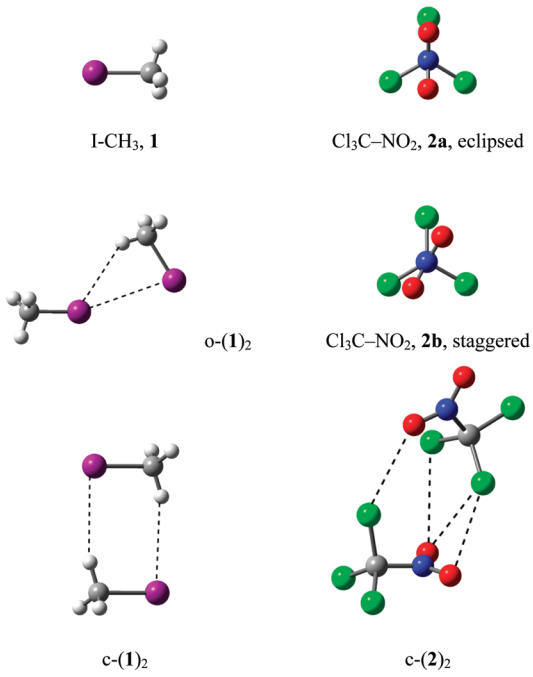

Figure 2. Molecular models of the optimized structures of methyl iodide **1**, chloropicrin **2**, and of some of their homodimers.

(d(C−I) = 2.160 Å; ∠(H−C−I) = 107.9°) agrees well with the experimental structure (d(C−I) = 2.139 Å; ∠(H−C−I) = 111.5°) determined by microwave spectroscopy.[52] Chloropicrin adopts an eclipsed structure **2a** in which one C−Cl bond and the NO_2 group are coplanar. The staggered structure **2b** is a transition state structure for rotation about the C−N bond (i24 cm^{-1}) with a relative free enthalpy of 1.4 kcal/mol. Barss studied the gas phase structure of chloropicrin by electron diffraction;[53] he determined the values d(C−Cl) = 1.75 ± 0.01 Å, ∠(Cl−C−Cl) = 110.8 ± 2.0°, and d(C−N) = 1.59 ± 0.04 Å and found the values d(N−O) = 1.21 Å and ∠(O−N−O) = 127° to be compatible with the observed intensities. The agreement with the computed values d(C−Cl) = 1.749 Å (1.754 Å (2×), 1.740 Å) and d(C−N) = 1.576 Å is very good, and the NO_2 parameters d(N−O) = 1.231 Å and ∠(O−N−O) = 128.1° also match closely. The computed ∠(Cl−C−Cl) angles (111.6° (2×), 111.5°) fall well within the experimental range, and molecular rotation in the gas phase would tend to reduce the ∠(Cl−C−Cl) angles slightly.

Electronic Structures and Electrostatic Potentials of Iodomethane and Chloropicrin. Mulliken and natural population analyses of the MP2(full)/6-31G* electron density of MeI show an almost neutral iodine, but the sign of q(I) depends on the method (MPA, −0.027; NPA, +0.064). Both methods agree that the C(δ^-)−H(δ^+) bonds are heavily polarized with positive q(H) values (MPA, +0.220; NPA, +0.255). The atom and group charges in chloropicrin show an overall electron withdrawing nitro group with $q(NO_2)$ values of −0.075 (MPA) and −0.159 (NPA) and strong internal quadrupolar charge distribution with high negative charges on both atoms (MPA, $q(O_{ecl})$ = −0.294, $q(O_b)$ = −0.292; NPA, $q(O_{ecl})$ = −0.299, $q(O_b)$ = −0.307). It is interesting and significant that the charges on the chlorine atoms are positive (MPA, $q(Cl_{ecl})$ = +0.132, $q(Cl_b)$ = +0119; NPA, $q(Cl_{ecl})$ = +0.109, $q(Cl_b)$ = +0.092), and their sum exceeds the overall CCl_3 group charge. In **2** it is beneficial to place a small negative charge q(C) of −0.229 (MPA) or −0.134 (NPA) close to the highly electron-deficient nitro-N with its charge q(N) of +0.446 (MPA) and +0.447 (NPA).

Population analysis methods rely on the partitioning of the molecular electron density into atomic regions. The results of the population analyses are fully corroborated by an electrostatic potential (ESP) analysis which is based on the molecular electron density distribution and independent of any partitioning. We determined the electrostatic potentials around **1** and **2** using both the MP2 and the QCI electron densities, and the surface-mapped plots of the QCI analysis are shown in Figure 3. The plots expound in an impressive fashion the high negative electrostatic potential at the nitro-O atoms and the high positive electrostatic potential around the methyl group. Interestingly, the ESP analysis reveals important details in the halogen regions. Iodine carries a very small charge only and features regions of negative and positive electrostatic potential: there remains a ring of negative potential (orange), and positive ESP values occur only in a small region of the iodine surface which is opposite to the CH_3 group. The chlorine atoms are positively charged, and the ESP values are positive on the entire surface surrounding the chlorine atoms. As with iodine, the ESP maxima on the chlorine atoms occur on the R−X lines and opposite to R.

Electrostatics and Intermolecular Interactions. The intramolecular charge distributions and electrostatic potentials inform the following discussions of intermolecular interactions. An R−I···O contact is a genuine iodine bonding interaction because it involves the interaction between an organohalide R−X and the negatively charged nitro-O atom. The important features of an iodine bonding interaction are the presence of a high negative charge on the heteroatom in close proximity to the highly polarizable iodine atom, i.e., an interaction in which charge-induced polarization is a dominant term. If the iodine atom is somewhat positively charged, then there is an additional bonding contribution due to charge−charge attraction.

Strictly speaking, an R−I···Cl contact would be considered as an iodine bonding interaction if the iodoalkane were to interact

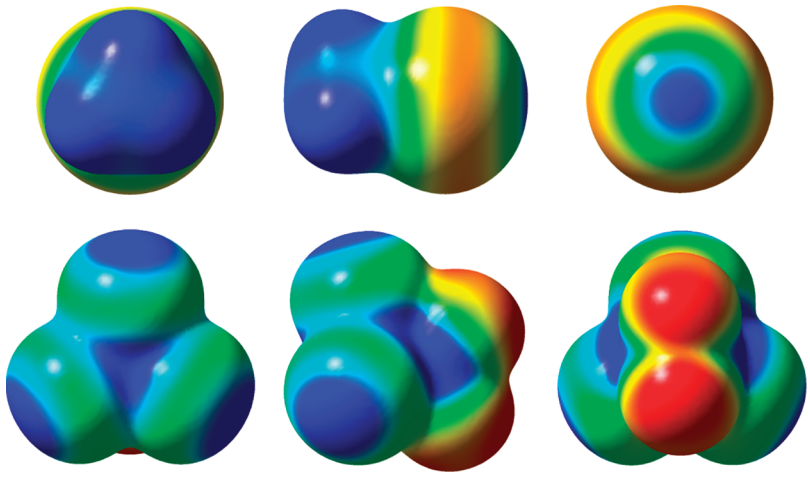

Figure 3. Electrostatic potentials mapped on the total electron density surfaces of methyl iodide **1** (top row) and chloropicrin **2**, respectively, computed with the QCI/6-31G* electron densities. Electrostatic potentials from −0.03 (red) to +0.03 (blue) and electron density surface computed for ρ = 0.002 e/au.[3]

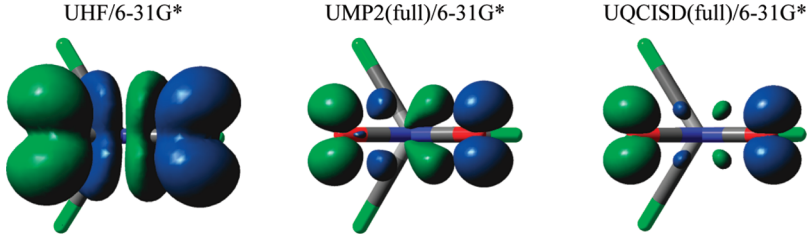

Atom: q; q^S	Atom: q; q^S	Atom: q; q^S
O_{ecl}: -0.331; +0.644	O_{ecl}: -0.413; -0.114	O_{ecl}: -0.337; -0.094
N: +0.458; 0.005	N: +0.645; 0.025	N: +0.501; +0.001
O_b: -0.321; -0.643	O_b: -0.425; +0.091	O_b: -0.339; +0.093
Cl_{ecl}: +0.140; -0.000	Cl_{ecl}: +0.153; +0.001	Cl_{ecl}: +0.146; +0.000
Cl_b: +0.120; -0.000	Cl_b: +0.144; -0.001	Cl_b: +0.133; -0.000

Figure 4. Spin density distributions of the singlet unrestricted wave functions of chloropicrin **2** computed at the levels UHF/6-31G*, UMP2(full)/6-31G*, and UQCISD(full)/6-31G* using the MP2(full)/6-31G* optimized structure. Surfaces are drawn for α and β spin density values of 0.004 e/au.[3] Atom charges (q) and spin populations (q^S) determined by Mulliken population analysis (MPA) for each electron density.

with a negatively charged Cl atom. In the present case, however, the Cl atoms are positively charged, and the positive charge is actually quite significant in magnitude. We suggest that the term iodine bonding remains applicable and beneficial if it is used in a more general, expanded sense for contacts that derive attraction from induced polarization whereby the inducing charge can be negative or positive.

Even though there is a tendency to focus on electrostatic interactions in discussion of halogen bonding (as with hydrogen bonding),[30] the bonding contribution from dispersion is large, and correlated methods are essential to correctly evaluate halogen bonding situations. Finally, one should distinguish between halogen bonding contacts and halogen−halogen contacts. The latter term refers to attractive interactions between identical or different halogen atoms in the absence of large molecular polarization and with dispersion being the main source of attraction.

Singlet Biradical Character of Chloropicrin. The RHF wave function of **2** exhibits a UHF instability and the unrestricted wave function of **2** is spin-polarized in a way that is reminiscent of ozone.[44] The spin density distributions computed at the UHF, UMP2, and UQCISD levels are shown in Figure 4, and the methods agree on the major features of the spin polarization. Opposite spin density accumulates on the oxygen atoms while the basin of the central nitrogen is spin-polarized but essentially without overall spin population.

The methods disagree however significantly with regard to the degree of spin polarization. The UHF method usually overestimates spin polarization because the method is prone to spin contamination, that is, the admixture of higher spin states and especially of the contribution from the next higher spin state s + 1 (triplet in the case of **2**). The employment of better correlation methods removes spin contamination successfully, and especially the UQCISD spin densities are of high quality. Note that the charge distribution patterns computed at all levels are in qualitative agreements and the MPA(UQCI) data show somewhat higher bond polarities.

Self-Aggregation of Iodomethane and Chloropicrin. The self-aggregation of methyl iodide[54] may involve iodine−iodine bonding (mainly dispersion) between two antiparallel and more or less collinear MeI molecules. However, an optimization starting from such a structure resulted in an open dimer o-$(\mathbf{1})_2$ (Figure 2) in which iodine of one molecule engaged in one iodine−iodine interaction (4.304 Å) and one iodine−hydrogen contact (3.359 Å, hydrogen-charge induced iodine polarization) with the other iodomethane. Another mode of MeI self-aggregation may involve two iodine−hydrogen contacts (3.306 Å) between two antiparallel and

dx.doi.org/10.1021/jf2037906 | J. Agric. Food Chem. 2012, 60, 1776−1787

side-by-side placed MeI molecules (dipole−dipole attraction). The resulting cyclic dimer c-$(\mathbf{1})_2$ is slightly preferred over the open dimer o-$(\mathbf{1})_2$.

As with MeI, the self-aggregation of chloropicrin likely involves the side-by-side placement of antiparallel oriented molecules to benefit from the dipole−dipole attraction. We constructed an initial structure with C_i-symmetry in which one chlorine of one molecule was oriented toward the nitro-N of the other and vice versa, i.e., one Cl of chloropicrin was in contact with both O atoms of the other chloropicrin. However, the optimization resulted in the asymmetric cyclic dimer c-$(\mathbf{2})_2$ shown in Figure 2. Dimer c-$(\mathbf{2})_2$ contains one eclipsed and one staggered chloropicrin, and the NO_2 planes are almost perpendicular with regard to each other while two CCl_2 planes remain essentially parallel. The arrangement allows for three Cl···O contacts: one between one O(NO_2) atom of the eclipsed molecule and one Cl of the staggered molecule (d(Cl···O) = 3.242 Å), and two contacts between the two O atoms of the NO_2 group of the eclipsed molecule and two chlorines of the staggered chloropicrin. The latter two contacts involve one chlorine bonding interaction in which Cl bridges between two O atoms ($d(Cl_a\cdots O_a)$ = 3.144 Å, $d(Cl_a\cdots O_b)$ = 3.377 Å) and one contact of another Cl with just one of the O atoms ($d(Cl_b\cdots O_b)$ = 3.561 Å). This arrangement leaves two C−Cl bonds of the two CCl_3 moieties pointing roughly in the same direction. Clearly, minimization of the aggregate dipole moment of c-$(\mathbf{2})_2$ is not a major driving force affecting the aggregate structure and, instead, halogen bonding is the structure maker.

Molecular Aggregates of Iodomethane and Chloropicrin. As shown in Figure 1, iodomethane may bind to chloropicrin with its iodine side and form iodine-bonded molecular aggregates (IBMA) or it may bind chloropicrin with its methyl side and form hydrogen-bonded molecular aggregates (HBMA). In addition, iodomethane may engage in iodine and hydrogen bonding at the same time and form IHBMA structures. Chloropicrin may engage in iodine or hydrogen bonding with one or both of its O atom(s) or with one or more of its Cl atoms.

We searched for all possible aggregates and located the IBMA structures **3** and **4** and the IHBMA structures **5** and **6** (Figure 5). Chloropicrin is eclipsed in all aggregates. In aggregates **3** and **4**, the CH_3 and CCl_3 groups are staggered with respect to each other. In the IBMA(O) structure **3**, iodine bridges asymmetrically between the O atoms ($d(I\cdots O_a)$ = 3.460 Å, $d(I\cdots O_b)$ = 3.791 Å, d(I···N) = 3.990 Å). In the IBMA(Cl) structure **4**, iodine is in contact with one Cl atom ($d(I\cdots Cl_a)$ = 4.001 Å, dashed in Figure 5) and considerably further away from the other chlorines ($d(I\cdots Cl_b)$ = 4.427 Å, $d(I\cdots Cl_c)$ = 4.506 Å, dotted in Figure 5).

In the IHBMA(O) structure **5**, one H atom bridges between the O atoms ($d(H\cdots O_a)$ = 2.681 Å, $d(H\cdots O_b)$ = 2.729 Å, d(H···N) = 2.986 Å) and iodine also bridges both O atoms ($d(I\cdots O_a)$ = 3.611 Å, $d(I\cdots O_b)$ = 3.630 Å). In structure **6**, two H atoms are in contact with two Cl atoms ($d(H_a\cdots Cl_a)$ = 3.150 Å, $d(H_b\cdots Cl_b)$ = 3.511 Å), and iodine is in contact with the third Cl atom ($d(I\cdots Cl_c)$ = 4.150 Å). Considering the charge distributions and electrostatic potentials of **1** and **2**, one must deduce that the attractive feature of **6** is hydrogen-charge induced chlorine polarization rather than classical hydrogen bonding (which requires negatively charged chlorine).

Stabilities of Homodimers vs Heterodimers. The ΔE data in Table 2 show that the reaction energies for the formation of the homodimers c-$(\mathbf{1})_2$ and c-$(\mathbf{2a})_2$ and of the mixed aggregate **3**−**6** are slightly negative; all dimers are bound on their respective energy surfaces. The contacts of MeI formed with O(**2**) are preferred over the contacts with Cl(**2**), and the formation of IHBMA **5** is best. Of course, aggregation reduces the rotational and translational freedom of the aggregated species, the reaction entropy is negative for aggregate forming reactions, and hence, the $-T\cdot\Delta S$ terms will be positive. We find that the entropy terms overwhelm the binding enthalpies for all homo- and heterodimers: the computed free enthalpies ΔG_{298} and $\Delta G'$ of the aggregations all are positive, and, hence, none of these aggregates are stable in the gas phase.

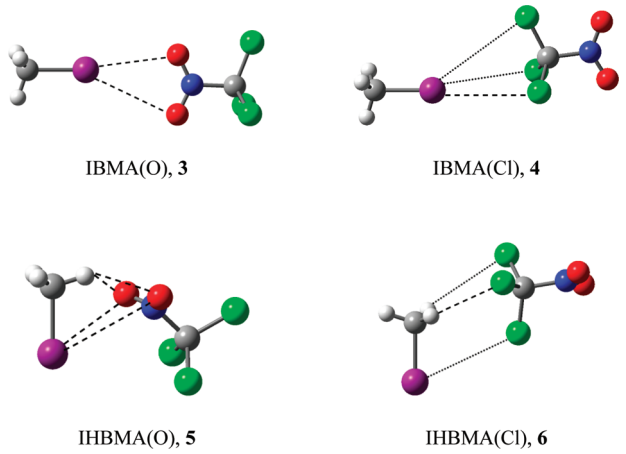

Figure 5. Models of the optimized structures of molecular aggregates formed between chloropicrin and CH_3I. Dashed and dotted lines indicate major and minor intermolecular contacts, respectively.

The benefits of mixed aggregation in solution are less affected by entropy effects because **1** and **2** engage in self-aggregation in their pure liquids. Liquids are highly dynamic systems, and the environment around each one molecule constantly changes. At all times, however, every molecule in a pure liquid is surrounded by a number of molecules of the same type. Any pair of molecules may assume a variety of configurations, and the optimized homodimer structures are the ones that are energetically preferred and they occur most often. In a liquid mixture, every molecule is surrounded by a number of molecules of two kinds, and these pairs also adopt a variety of configurations. For any pair of different molecules, the optimized heterodimer structures are the energetically preferred configurations and they occur most often. We are primarily interested in the difference of the free enthalpies of homodimers and heterodimers. A higher stability of the heterodimers compared to the homodimers provides strong evidence for reduced volatility of the liquid mixture. In the simplest model, one can consider the homodimers and evaluate the reactions that convert one homodimer of **1** and one homodimer of **2** to two mixed aggregates of **1** and **2**. We computed the respective values for heterodimers **3**−**6**, and they are also listed in Table 2. Note that all of the reaction energies listed in Table 2 are based on the formation of one mixed aggregate. With reference to the homodimers, the formations of **3**−**5** are found to be exergonic while the formation of **6** remains slightly endergonic. The iodine-bonded structures **3** and **4** are almost isoenergetic (ΔG_{form} = −1.9 kcal/mol) and bound significantly more than the hydrogen-bonded aggregate **5** (ΔG_{form} = −0.8 kcal/mol).

dx.doi.org/10.1021/jf2037906 | J. Agric. Food Chem. 2012, 60, 1776−1787

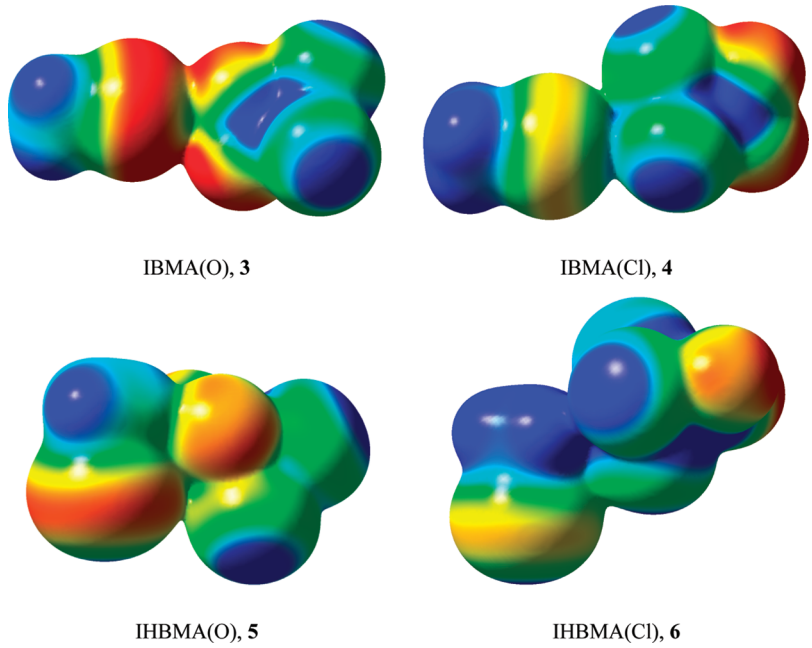

Figure 6. Electrostatic potentials mapped on the total electron density surfaces of aggregates **3**–**6** computed with the QCI/6-31G* electron densities. Electrostatic potentials from −0.03 (red) to +0.03 (blue) and electron density surface computed for 0.002 e/au.[3] Molecules are oriented as shown in Figure 5.

It is important to note that the binding of the most stable mixed aggregates **3** and **4** is due to the entropy terms and that this binding occurs in spite of the fact that self-aggregation would provide more binding enthalpy. Conversely, mixed aggregate **5** has the highest binding energy with regard to free monomers (ΔE = −4.0 kcal/mol) and its binding energy remains negative with regard to the homodimers (ΔE = −1.1 kcal/mol). However, the high binding energies of **5** are achieved only with a high degree of structural order and at the expense of its molecular entropy.

The analysis of the differences $\Delta\Delta E = \Delta E' - \Delta E$ is highly instructive. The $\Delta\Delta E$ values are usually positive and less than 0.5 kcal/mol but the $\Delta\Delta E$ values for one system stand out. For the formation of aggregate **4**, the $\Delta\Delta E$ values are negative and greater than unity in magnitude and show that the iodine–chlorine contact in **4** greatly benefits from dispersion. It is this dispersion effect on the binding of **4** that changes the stability ranking based on the $\Delta G'_{form}$ values as compared to the ΔG_{form} data: **4** ($\Delta G'_{form}$ = −3.6 kcal/mol) > **3** (−2.0 kcal/mol) > **5** (−0.7 kcal/mol).

Methyl Group Rotations in Iodine-Bonded Aggregates 3 and 4. The thermochemical data listed in Table 1 are computed with the harmonic approximation and assuming that even the low-frequency modes are bona fide vibrations. However, aggregates **3** and **4** contain one internal degree of freedom that corresponds to an essentially free methyl group rotation, and the treatment of this internal rotation as a vibration may add considerable error to the thermochemical data. Hence, we computed the thermochemistry of **3** and **4** again with proper accounting for the internal methyl rotation (instead of vibration ν_1) using the method by Ayala and Schlegel,[41b] and the resulting TE_{HR} and S_{HR} values are included in Table 1 in the second rows for **3** and **4**.

The proper treatment of the internal hindered rotors reduces the thermal energies and the molecular entropies of **3** and **4**. The lowered value of TE_{HR} increases the stability of the aggregate. On the other hand, the ΔS values for the formation of **3** and **4** are negative since $S(\mathbf{3})$ and $S(\mathbf{4})$ are smaller than the sum of $S(\mathbf{1})$ and $S(\mathbf{2b})$, the ΔS values become more negative with the hindered rotor thermochemistry, and, hence, the free enthalpy of formation becomes less negative. The overall consequences are that the values $\Delta G'_{f,HR}(\mathbf{3})$ and $\Delta G'_{f,HR}(\mathbf{4})$ are slightly reduced to −1.3 and −2.5 kcal/mol, respectively.

Aggregation Effects on Electrostatic Potentials. We performed Mulliken population analyses (MPA) and computed electrostatic potentials with the QCI electron density distributions to assess the electronic relaxation associated with the formation of aggregates **3**–**6**. In Figure 6 are shown the electrostatic potentials mapped on isosurfaces of the total electron densities, and the results of the population analysis are provided in Table 3 in the Supporting Information.

Aggregation reduces the negative charge on the NO_2 group, increases the positive charge of the CCl_3 group, and causes a small transfer of electron density to CH_3I. These changes are negligible for **4** and **6**, while the intermolecular charge transfer is on the order of 0.02–0.03 electron for **3** and **5** and causes noticeable differences in the electrostatic properties in the iodine region of **3** and **5** (Figure 6) compared to the respective plots of the free molecules **1** and **2** (Figure 2). The ESP plots show the ring of negative potential around iodine to be enhanced in **3** and **5**.

Addition Chemistry of Iodomethane and Chloropicrin. The addition of **1** to the NO_2 group of **2** may involve either 1,2- or 1,3-addition and lead to **7** or **8**, respectively. Both addition products correspond to stable minima (Figure 7): **7** is the *N*-oxide of *N*-iodo-*N*-methoxytrichloromethyl-amine (d(N–I) = 2.593 Å), **8** is a hydroxylamine derivative (d(O–I) = 2.548 Å), and the thermodynamic stabilities of **7** and **8** are similar with only a small preference of ΔG_{rel} = 1.2 kcal/mol for **7** over **8** (Table 2) at the level of optimization. Isomers **7** and **8** are connected by the transition state structure TS(**7**,**8**) for 1,2-iodine shift, and the activation barriers (ΔG_{act}) for the forward

dx.doi.org/10.1021/jf2037906 | J. Agric. Food Chem. 2012, 60, 1776–1787

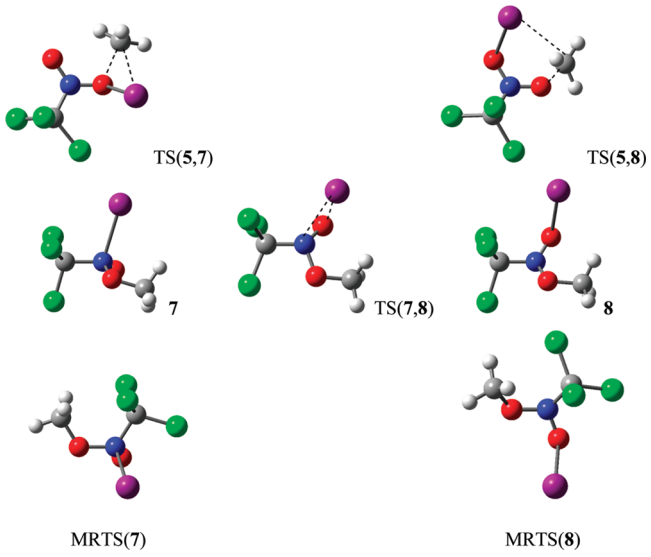

Figure 7. Models of the optimized structures of products 7 and 8 of addition of CH_3I to chloropicrin and of transition state structures for their formation TS(5,7) and TS(5,8), for product isomerization TS(7,8), and for automerizations of 7 and 8.

and backward reactions of the isomerization 7 ⇄ 8 are 27.1 and 26.0 kcal/mol, respectively. The CCl_3 and CH_3 groups in 7 and 8 are essentially trans with regard to the NO bond, and the respective cis conformations are transition state structures MRTS(7) and MRTS(8) for methyl rotation about the NO bonds in 7 and 8, respectively. Significant steric crowding in the cis structures results in activation barriers of more than 15 kcal/mol (Table 2).

The stability tests for 7, 8, and TS(7,8) reveal UHF instabilities for all three structures, and the spin density distributions of the optimized and spin-polarized singlet wave functions (Figure 9 in Supporting Information) contain some radical pair character $[2+CH_3]^{\bullet}$ $[I]^{\bullet}$ with α-spin on iodine and β-spin on the NO moiety. The large and extended spin-polarizations underscore the need for the energy computations at the UQCISD(full)/6-31G*//MP2(full)/6-31G* level. Compound 8 benefits from the higher level correlation methods more than 7, and the isomer preference is reversed in favor of 8 ($\Delta G'_{rel}$ = 5.0 kcal/mol). The more complete correlation computations benefit the less bonded TS(7,8) more than either minimum, and, hence, the activation free enthalpies ($\Delta G'_{act}$) for the forward and backward reactions of the isomerization 7 ⇄ 8 drop to 11.8 and 16.8 kcal/mol, respectively.

The reactions 1 + 2a → 7 and 1 + 2a → 8 are endothermic and endergonic and, hence, 7 and 8 will not accumulate in any significant amounts, but they are plausible reactive intermediates on the way to thermodynamically more stable species. As with the aggregation energies discussed above, the consideration of self-aggregation of 1 and 2 has a pronounced effect on the reaction thermodynamics. While self-aggregation increases the activation energies by about 3 kcal/mol, it also has the effect of reducing the reaction free enthalpies by ca. 5.5 kcal/mol, and the $\Delta G'$ values for the formations of 7 and 8, respectively, are 30.7 and 25.7 kcal/mol, respectively.

Fragmentation Reactions of the Addition Products. Assuming that 7 and 8 might be accessible as reactive intermediates even in very tiny concentrations, one can imagine a number of possible reaction channels for fragmentation (Figure 8). The addition of H_3C-I to chloropicrin followed by elimination of Cl_3C-I, 9, results overall in the conversion of the nitro compound 2 to methyl nitrite, 10. This outcome can be achieved by α-elimination from 7 or by β-elimination from 8. A second possible outcome consists in the formation of 1,1,1-trichloroethane, 11, by β-elimination from 7 or 8, respectively, and leading to $I-NO_2$, 12, or IO−NO, 13, respectively. A third possibility would be the formation of trichloromethyl methyl ether, 14, by α-elimination from 7 or 8, respectively, and leading to I−N═O, 15, or I−ON, 16, respectively. Finally, there exists the possibility for β-elimination from 8 leading to $Cl_3C-N{=}O$, 17, and iodosomethane, $IO-CH_3$, 18. The products of these reactions are known and well-characterized species with the exception of isonitrosyl iodide, 16, and the hypoiodous acid ester 18. Isonitrosyl halides X−ON have been described[55] for X = Cl, Br but not yet for X = I. The methyl ester of hypoiodous acid IO−

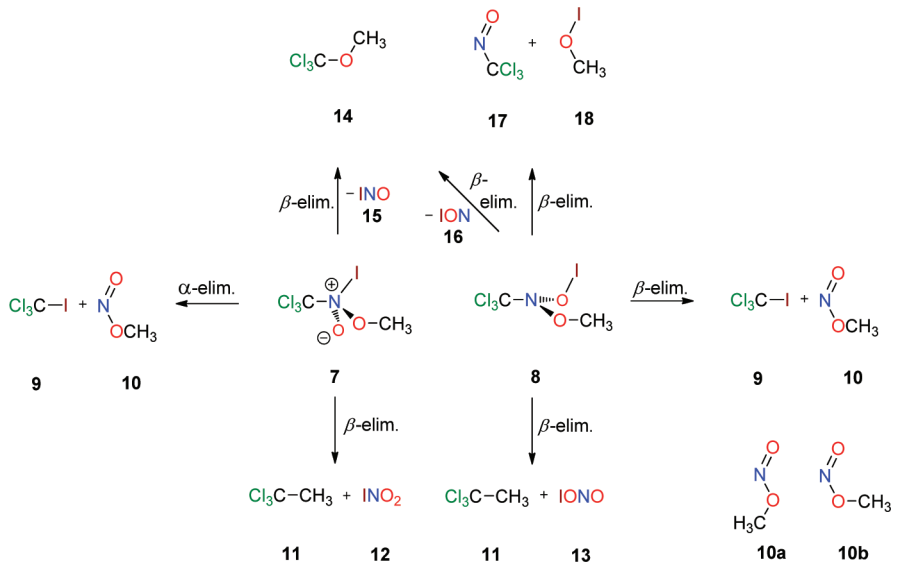

Figure 8. Fragmentation paths for primary addition products 7 and 8.

dx.doi.org/10.1021/jf2037906 | J. Agric. Food Chem. 2012, 60, 1776–1787

CH_3, **18**, has been studied theoretically in the context of direct oxidation of MeI.[56]

We computed the structures of **9**−**18**, models of their structures are provided in Figure 10 as part of the Supporting Information, their energies are listed in Table 1, and relative and reaction energies are provided in Table 2. At the level of optimization, methyl nitrite prefers the s-cis structure **10b** over the s-trans structure **10a** by ΔG_{rel} = 1.7 kcal/mol.[57] Nitrosyl hypoiodite prefers the s-cis structure **13b** over the s-trans structure **13a** by ΔG_{rel} = 4.7 kcal/mol, and the nitryl iodide isomer, **12**, is preferred over **13b** by another ΔG_{rel} = 2.4 kcal/mol. Nitrosyl iodide I−N═O, **15**, is much preferred over isonitrosyl iodide I−ON, **16**, by ΔG_{rel} = 15.9 kcal/mol. The isomer stabilities of **10** ($\Delta G'_{rel}$ = 1.4 kcal/mol) and **13** ($\Delta G'_{rel}$ = 4.6 kcal/mol) are essentially the same at the UQCISD level. But the higher level energies indicate a reversal of the relative stabilities of INO_2 (**12**) and IONO (**13**) with a preference of $\Delta G'_{rel}$ = 7.0 kcal/mol in favor of **13b**. The preference for **15** over **16** persists at the QCI level although it is greatly diminished to $\Delta G'_{rel}$ = 8.8 kcal/mol. The cis preference of **13** agrees with previous studies.[58,59] A preference for **12** over **13** was reported based on effective core potential computations at MP2, B3LYP, and CCSD(T)/B3LYP levels.[59] The reversal of the stabilities of **12** and **13** at the UQCISD(full)/6-31G* level is primarily a consequence of the all-electron CI treatment, and the use of the unrestricted reference wave function in the CI treatment enhances the reversal by another 2 kcal/mol.

We are interested in the reaction energies of the five fragmentation reactions listed in Table 2, and all of these values are based on the most stable isomer of each species. At the level of optimization, only the two fragmentation channels **B** and **D** of **7** lead to products that are thermodynamically more stable than substrates **1** and **2**. But here again, the recognition and adequate accounting for spin polarization proves crucial and the additional stabilization of the fragmentation products **10**, **13**, **15**−**17** drives reactions **A** and **C**−**D** substantially to the right and renders reactions **A**−**D** exothermic (Table 2). The sequence **1** + **2a** → **9** + **10b** is exergonic by $\Delta G'(\mathbf{A})$ = −4.5 kcal/mol, reaction **1** + **2a** → **11** + **12** is exergonic by $\Delta G'(\mathbf{B})$ = −5.5 kcal/mol, the reaction **1** + **2a** → **11** + **13** is exergonic by $\Delta G'(\mathbf{C})$ = −13.2 kcal/mol, and the sequence **1** + **2a** → **14** + **15** is exergonic by $\Delta G'(\mathbf{D})$ = −23.9 kcal/mol.

Kinetic Accessibility of Addition Products. The reaction transition state structures[60] TS(**5**,**7**) and TS(**5**,**8**) were located for the 1,2- and 1,3-additions of MeI to chloropicrin, respectively, and they are shown in Figure 7. The TS(**5**,**7**) structure shows an overall almost neutral MeI with an elongated and heavily polarized MeI bond (2.839 Å) oriented to place its methyl moiety close to one nitro-O (1.967 Å). The mechanism of this addition is basically a methyl transfer from I to O and N−I bond formation is a secondary event on the downhill side. In sharp contrast, the O−I bond formation on the way to **8** occurs early and well before the transition state structure is reached. The O−I bond (2.528 Å) is fully formed in the TS(**5**,**8**) structure (it is shorter than in **8**), and the N-pyramidalization has progressed significantly as the methyl transfer from I (2.915 Å) to O (2.144 Å) occurs. The spin density distributions of TS(**5**,**7**) and TS(**5**,**8**) show dissociating, spin-polarized iodomethane in association with heavily spin-polarized NO_2 groups (Figure 9 in Supporting Information).

The homolytic bond dissociation energy of iodomethane $D(H_3C{-}I)$ = 56.4 kcal/mol was measured.[61,62] The homolytic bond dissociation energy of chloropicrin $D(Cl_3C{-}NO_2)$ = 41.7 kcal/mol was determined at a high level of theory,[63] and the radical-induced degradation of chloropicrin (i.e., by $HO^{\bullet}$) becomes important even below this threshold.[64] Consequently, any thermal one-step reaction path with an activation energy above 40 kcal/mol would be disadvantaged as compared to a multistep radical path to the same product.

The computed activation barriers ($\Delta G'_{act}$) for the formations of **7** and **8**, respectively, are 82.4 and 79.2 kcal/mol, respectively. Thus, one can safely conclude that the direct additions of **1** to **2** will not occur, while the stepwise additions of methyl radical and of iodine to chloropicrin present possible paths to **7** and **8**, respectively, as well to the radical pairs $[\mathbf{2}{+}CH_3]^{\bullet}$ $[I]^{\bullet}$ and/or $[\mathbf{2}{+}I]^{\bullet}$ $[CH_3]^{\bullet}$. But any of these paths would still require activation energy on the order of 50 kcal/mol for the formation of the reactive intermediate(s) and suffer from substrate depletion, and any such chemistry would be slow and unproductive.

Conclusions. In conclusion, the name methyl iodide does not capture the actual polarity of iodomethane. Iodine in CH_3−I is certainly nothing like "iodide" and instead it is close to neutral. The electronic structure of chloropicrin is dominated by the negatively charged nitro group which causes significant positive charges on the chlorine atoms.

Self-aggregation of iodomethane involves iodine−iodine contacts (mostly dispersion) and hydrogen bonds to iodine (hydrogen-charge induced iodine polarization). Self-aggregation of chloropicrin involves a number of chlorine−oxygen contacts. These Cl···O contacts benefit from charge−charge attraction between $Cl(\delta^+)$ and $O(\delta^-)$ and from chlorine bonding (oxygen-charge induced chlorine polarization).

Two iodine-bonded molecular aggregates can be formed by aggregation of iodomethane and chloropicrin. Aggregate **3** involves genuine iodine bonding (oxygen-charge induced iodine polarization), and aggregate **4** involves some iodine bonding in the broader sense (chlorine-charge induced iodine polarization) and significant iodine−chlorine bonding (dispersion). Aggregates **5** and **6** with hydrogen bonding between methyl-Hs of iodomethane and chloropicrin's O or Cl acceptors exist on the potential energy surface. Aggregate **5** also features some iodine bonding, and **5** remains bound on the free enthalpy surface while **6** does not.

The mixed aggregates **3**−**5** are bound on the free enthalpy surface relative to the homodimers of **1** and **2**. This result suggests that the liquid mixture of chloropicrin and iodomethane is a good choice to reduce the volatilities of iodomethane and chloropicrin because of thermodynamically stabilizing intermolecular iodine bonding.

Mixtures of iodomethane and chloropicrin are not expected to show chemistry resulting from their reactions with each other. All of the paths involving the addition products **7** and **8** and/or the radical pairs $[\mathbf{2}{+}CH_3]^{\bullet}$ $[I]^{\bullet}$ and/or $[\mathbf{2}{+}I]^{\bullet}$ $[CH_3]^{\bullet}$ as intermediates require activation energies in excess of 50 kcal/mol, and any such thermal chemistry is unproductive.

■ ASSOCIATED CONTENT

Ⓢ Supporting Information

Theoretical level dependency of potential-mapped total electron density surfaces of **1** and **2** (Figure 3, expanded), spin density distributions of **7**, **8**, TS(**5**,**7**), TS(**5**,**8**), and TS(**7**,**8**) (Figure 9), models of the optimized structures of **9**−**18** (Figure 10), results of QCI Population Analysis of **1**−**6** (Table 3), Cartesian coordinates of stationary structures, total energies computed at various levels of perturbation theory, and

an expanded discussion of the relative stabilities of **12** and **13**. This material is available free of charge via the Internet at http://pubs.acs.org.

AUTHOR INFORMATION

Corresponding Author

*Phone: (593) 882-0331. E-mail: glaserr@missouri.edu.

Funding

MU Research Computing is supported by NASA Funding and additional support from Dell, SGI, Sun Microsystems, TimeLogic, and Intel. K.P. is the recipient of a 2011 Arts and Science Undergraduate Research Mentorship.

Notes

The authors declare no competing financial interest.

REFERENCES

(1) U. S. Environmental Protection Agency. The Phase-out of Methyl Bromide. http://www.epa.gov/ozone/mbr/ (accessed 8/24/2011).

(2) Kley, D.; Crutzen, P. J.; Smit, H. G. J.; Vömel, H.; Oltmans, S. J.; Grassl, H.; Ramanathan, V. Observations of Near-Zero Ozone Concentrations Over the Convective Pacific: Effects on Air Chemistry. *Science* **1996**, *274*, 230−233.

(3) U. S. Environmental Protection Agency. Methyl Bromide Alternatives. http://www.epa.gov/ozone/mbr/alts.html (accessed 8/24/2011).

(4) (a) U. S. Environmental Protection Agency. Extension of Conditional Registration of Iodomethane (Methyl Iodide). Online at http://www.epa.gov/pesticides/factsheets/iodomethane_fs.htm (accessed 8/24/2011). (b) Erickson, B. E. Methyl Iodide Saga Continues. EPA gives green light to soil fumigant, but California is still Assessing Risks. *Chem. Eng. News* **2008**, *86*, 28−30.

(5) U. S. Environmental Protection Agency. Press Release on Pesticides and Toxic Chemicals. Soil Fumigant Pesticides Subject to New Safety Measures. July 10, 2008. Online at http:// http://www.epa.gov/newsroom/newsreleases.htm#subject (accessed 8/24/2011).

(6) Pelley, J. Methyl iodide, a fumigant under fire. *Environ. Sci. Technol.* **2009**, *43*, 6898.

(7) Rubin, S.; Schmalz, D. The Midas Touch, The Midas Effect. *Monterey County Weekly*. March 10, **2011**. Online at http://www.montereycountyweekly.com/news/2011/mar/10/midas-touch-midas-effect/ along with hyperlinks to background materials (accessed 8/24/**2011**).

(8) Kirman, C. R.; Sweeney, L. M.; Gargas, M. L.; Kinzell, J. H. Evaluation of possible modes of action for acute effects of methyl iodide in laboratory animals. *Inhalation Toxicol.* **2009**, *21*, 537−551.

(9) Bolt, H. M.; Gansewendt, B. Mechanisms of carcinogenicity of methyl halides. *Crit. Rev. Toxicol.* **1993**, *23*, 237−253.

(10) McFiggans, G.; Plane, J. M. C.; Allan, B. J.; Carpenter, L. J.; Coe, H.; O'Dowd, C. A. Modeling study of iodine chemistry in the marine boundary layer. *J. Geophys. Res.* **2000**, *105*, 14371−14385.

(11) Platt, U.; Honninger, G. The role of halogen species in the troposphere. *Chemosphere* **2003**, *52*, 325−338.

(12) Hughes, C. H.; Franklin, D. J.; Malin, G. Iodomethane production by two important marine cyanobacteria: Prochlorococcus marinus (CCMP 2389) and Synechococcus sp. (CCMP 2370). *Mar. Chem.* **2011**, *125*, 19−25.

(13) Toda, H.; Itoh, N. Isolation and characterization of a gene encoding a *S*-adenosyl-*L*-methionine-dependent halide/thiol methyltransferase (HTMT) from the marine diatom Phaeodactylum tricornutum: Biogenic mechanism of CH_3I emissions in oceans. *Phytochemistry* **2011**, *72*, 337−343.

(14) Rhew, R. C.; Ostergaard, L.; Saltzman, E. S.; Yanofsky, M. F. Genetic Control of Methyl Halide Production in Arabidopsis. *Curr. Biol.* **2003**, *13*, 1809−1813.

(15) (a) Jones, C. E.; Hornsby, K. E.; Sommariva, R.; Dunk, R. M.; von Glasow, R.; McFiggans, G.; Carpenter, L. J. Quantifying the contribution of marine organic gases to atmospheric iodine. *Geophys. Res. Lett.* **2010**, *37*, L18804/1−L18804/6. (b) Wang, L.; Moore, R. M.; Cullen, J. J. Methyl iodide in the NW Atlantic: spatial and seasonal variation. *J. Geophys. Res.* **2009**, *114*, C07007/1−C07007/13.

(16) (a) Bland, P. A.; Bevan, A. W. R.; Jull, A. J. T. Ancient Meteorite Finds and the Earth's Surface Environment. *Quat. Res.* **2000**, *53*, 131−142. (b) Heumann, K. G.; Gall, M.; Weiss, H. Geochemical investigations to explain iodine-overabundances in Antarctic meteorites. *Geochim. Cosmochim. Acta* **1987**, *51*, 2541−2547.

(17) Kollman, W. S.; Barry, T. S.; Spurlock, F. Environmental Fate of Iodomethane, Department of Pesticide Regulation, Environmental Monitoring Branch: P.O. Box 4015 Sacramento, California 95812−4015, Aug 2009.

(18) (a) Gan, J.; Yates, S. R. Degradation and Phase Partition of Methyl Iodide in Soil. *Agric. Food Chem.* **1996**, *44*, 4001−4008. (b) Zheng, W.; Papiernik, S. K.; Guo, M.; Yates, S. R. Accelerated Degradation of Methyl Iodide by Agrochemicals. *J. Agric. Food Chem.* **2003**, *51*, 673−679. (c) Luo, L.; Ashworth, D.; Dungan, R. S.; Xuan, R.; Yates, S. R. Transport and Fate of Methyl Iodide and Its Pest Control in Soils. *Environ. Sci. Technol.* **2010**, *44*, 6275−6280.

(19) Woodrow, J. E.; Seiber, J. N.; Miller, G. C. Correlation To Estimate Emission Rates for Soil-Applied Fumigants. *J. Agric. Food Chem.* **2011**, *59*, 939−943.

(20) (a) Ashworth, D. J.; Ernst, F. F.; Xuan, X.; Yates, S. R. Laboratory assessment of emission reduction strategies for the agricultural fumigants 1,3-dichloropropene and chloropicrin. *Environ. Sci. Technol.* **2009**, *43*, 5073−5078. (b) Gao, S.; Qin, R.; Hanson, B. D.; Tharayil, N.; Trout, T. J.; Wang, D.; Gerik, J. Effects of Manure and Water Applications on 1,3-Dichloropropene and Chloropicrin Emissions in a Field Trial. *J. Agric. Food Chem.* **2009**, *57*, 5428−5434.

(21) Ashworth, D. J.; Luo, L.; Xuan, R.; Yates, S. R. Irrigation, Organic Matter Addition, and Tarping As Methods of Reducing Emissions of Methyl Iodide from Agricultural Soil. *Environ. Sci. Technol.* **2011**, *45*, 1384−1390.

(22) Gao, S.; Qin, R.; McDonald, J. A.; Hanson, B. D.; Trout, T. J. Field tests of surface seals and soil treatments to reduce fumigant emissions from shank injection of Telone C35. *Sci. Total Environ.* **2008**, *405*, 206−214.

(23) (a) Kollman, W. S.; Barry, T. A.; Spurlock, F. Methyl Iodide (Iodomethane) Risk Characterization Document For Inhalation Exposure. *Env. Monitoring Branch, Dept. Pesticide Regulation, California Env. Protection Agency* **2009**, *3*, 1−19. (b) Henry's law constant specifies the concentration ratio of a compound distributed between air and aqueous solution.

(24) Niyaz, N.; Tisdell, F. E.; Watson, G. B.; Renga, J. M.; Lo, W. C.; Yap, M. C. H. *Insecticidal Pyridine Compounds*. International Patent WO 2010/126580, Nov. 4, 2010.

(25) Bowles, V. M.; Macleman, P. Combination Compositions and Methods of Use of the Same for Controlling Infestation. International Patent WO 2009/047584, Apr. 16, 2009.

(26) For an example of mixing MeI with a *more* volatile liquid, see: Poss, A. J.; Singh, R. R.; Pham, H. T. Azeotropic fumigant compositions and methods of controlling pests. U.S. Pat. Appl. Publ. 2010, US 2010/0135914 A1, June 3, 2010. The azeotropic mixture of MeI and sulfuryl fluoride (SO_2F_2) is used as a highly volatile fumigant.

(27) (a) Arysta LifeScience. Online at http://www.arystalifescience.com (accessed 8/24/2011). (b) Material Safety Data Sheets for various MIDAS formulations are available online at http://www.midas-therightfoundation.com (accessed 8/24/2011).

(28) Sparks, S. E.; Quistad, G. B.; Li, W.; Casida., J. E. Chloropicrin Dechlorination in Relation to Toxic Action. *J. Biochem. Mol. Toxicol.* **2000**, *14*, 26−32.

(29) (a) Parisini, E.; Metrangolo, P.; Pilati, T.; Resnati, G.; Terraneo, G. Halogen bonding in halocarbon-protein complexes: a structural survey. *Chem. Soc. Rev.* **2011**, *40*, 2267−2278. (b) Cavallo, G.; Metrangolo, P.; Pilati, T.; Resnati, G.; Sansotera, M.; Terraneo, G. *Chem. Soc. Rev.* **2010**, *39*, 3772−3783. (c) Fourmigue, M. Halogen bonding: Recent advances. *Curr. Opin. Solid State Mater. Sci.* **2009**, *13*,

36−45. (d) Brammer, L.; Espallargas, G. M.; Libri, S. Combining metals with halogen bonds. *CrystEngComm* **2008**, *10*, 1712−1727.
(30) Politzer, P.; Murray, J. S.; Clark, T. Halogen bonding: an electrostatically-driven highly directional noncovalent interaction. *Phys. Chem. Chem. Phys.* **2010**, *12*, 7748−7757.
(31) (a) Glaser, R. Polar Order By Rational Design: Crystal Engineering With Parallel Beloamphiphile Monolayers. *Acc. Chem. Res.* **2007**, *40*, 9−17. (b) Glaser, R.; Murphy, R. F. What's in a name? Noncovalent Ar−Cl···$(H-Ar')_n$ interactions and terminology based on structure and nature of the bonding. *CrystEngComm* **2006**, *8*, 948−951. (c) Glaser, R.; Chen, N.; Wu, H.; Knotts, N.; Kaupp, M. ^{13}C-NMR Study of Halogen Bonding of Haloarenes. Measurement of Solvent Effects and Theoretical Analysis. *J. Am. Chem. Soc.* **2004**, *126*, 4412−4419. (d) Glaser, R.; Knotts, N.; Wu, H. Polar Order in Crystalline Molecular Organic Materials by Rational Design. *Chemtracts* **2003**, *16*, 443−452.
(32) Mudadu, M. S.; Singh, A.; Thummel, R. P. 7-Pyridylindoles: Synthesis, Structure, and Properties. *J. Org. Chem.* **2006**, *71*, 7611−7617.
(33) Nagasako, T.; Ogata, T.; Kurihara, S.; Nonaka, T. Synthesis of Thermosensitive Copolymer Beads Containing Pyridinium Groups and Their Antibacterial Activity. *J. Appl. Polym. Sci.* **2010**, *116*, 2580−2589.
(34) Ujiie, S.; Tanaka, Y.; Iimura, K. Thermal Behavior of Ionic liquid-Crystalline Side-Chain Polymer. *Mol. Cryst. Liq. Cryst.* **1993**, *225*, 399−402.
(35) Reid, B. L.; Baker, R. B.; Bao, N. N.; Koufas, D. A.; Kent, G. J.; Baur, P. Synergistic pesticide compositions containing adjuvants. U.S. Pat. Appl. Publ. 2010, US2010/0247684 A1, Sept 30, 2010.
(36) Cramer, C. J. *Essentials of Computational Chemistry: Theories and Models*, 2nd ed.; Wiley: Chichester, 2004.
(37) Shavitt, I.; Bartlett, R. J. *Many-Body Methods in Chemistry and Physics: MBPT and Coupled-Cluster Theory*; Cambridge University Press: Cambridge, U.K., 2009.
(38) (a) Hehre, W. J.; Ditchfield, R.; Pople, J. A. Self-consistent molecular orbital methods. XII. Further extensions of Gaussian-type basis sets for use in molecular orbital studies of organic molecules. *J. Chem. Phys.* **1972**, *56*, 2257−2261. (b) Francl, M. M.; Petro, W. J.; Hehre, W. J.; Binkley, J. S.; Gordon, M. S.; DeFrees, D. J.; Pople, J. A. Self-consistent molecular orbital methods. XXIII. A polarization-type basis set for second-row elements. *J. Chem. Phys.* **1982**, *77*, 3654−3665.
(39) Glukhovstev, M. N.; Pross, A.; McGrath, M. P.; Radom, L. Extension of Gaussian-2 (G2) theory to bromine- and iodine-containing molecules: use of effective core potentials. *J. Chem. Phys.* **1995**, *103*, 1878−1885.
(40) Peng, C.; Ayala, P. Y.; Schlegel, H. B.; Frisch, M. J. Using redundant internal coordinates to optimize equilibrium geometries and transition states. *J. Comput. Chem.* **1996**, *17*, 49−56.
(41) (a) McClurg, R. B.; Flagan, R. C.; Goddard, W. A. III. The hindered rotor density-of-states interpolation function. *J. Chem. Phys.* **1997**, *106*, 6675−6680. (b) Ayala, P. Y.; Schlegel, H. B. Identification and treatment of internal rotation in normal mode vibrational analysis. *J. Chem. Phys.* **1998**, *108*, 2314−2325.
(42) Schlegel, H. B.; McDouall, J. J. In *Computational Advances in Organic Chemistry*; Ögretir, C., Csizmadia, I. G., Eds.; Kluwer Academic: The Netherlands, 1991; pp 167−185.
(43) (a) Hollett, J. W.; Gill, P. M. W. The two faces of static correlation. *J. Chem. Phys.* **2011**, *134*, 114111. (b) Lepetit, M. B.; Malrieu, J. P. Interaction of s^2 pairs in beryllium dimer and carbon dimer: the UHF instability, symptom of an atomic promotion. *Chem. Phys. Lett.* **1990**, *169*, 285−291.
(44) (a) Chan, W.-T.; Hamilton, I. P. Mechanisms for the ozonolysis of ethene and propene: Reliability of quantum chemical predictions. *J. Chem. Phys.* **2003**, *118*, 1688−1701. (b) Pulay, P.; Liu, R. F. Methods for finding unrestricted Hartree-Fock solutions and multiple solutions. *J. Phys. Chem.* **1990**, *94*, 5548−5551. (c) Highly correlated systems: structure, binding energy and harmonic vibrational frequencies of ozone. Raghavachari, K.; Trucks, G. W.; Pople, J. A.; Replogle, E. *Chem. Phys. Lett.* **1989**, *158*, 207−212.
(45) (a) Kuz'mitskii., V. A. Instability Of The Molecular Structure Of Monobenzoporphin To The Alternation Of The Macrocycle Bond Lengths And Its Manifestation In The Electronic Spectra. *J. Appl. Spectrosc.* **2004**, *71*, 777−787. (b) Colvin, M. E.; Janssen, C. L.; Seidl, E. T.; Nielsen, I. M. B.; Melius, C. F. Energies, resonance and UHF instabilities in polycyclic aromatic hydrocarbons and linear polyenes. *Chem. Phys. Lett.* **1998**, *287*, 537−541.
(46) (a) Sheka, E. F.; Chernozatonskii, L. A. Broken symmetry approach and chemical susceptibility of carbon nanotubes. *Int. J. Quant. Chem.* **2010**, *110*, 1466−1480. (b) Sheka, E. F. Chemical susceptibility of fullerenes in view of Hartree-Fock approach. *Int. J. Quant. Chem.* **2007**, *107*, 2803−2816.
(47) Bachrach, S. M. Population analysis and electron densities from quantum mechanics. *Rev. Comput. Chem.* **1994**, *5*, 171−227.
(48) Reed, A. E.; Weinstock, R. B.; Weinhold, F. Natural-population analysis. *J. Chem. Phys.* **1985**, *83*, 735−46.
(49) (a) Murray, J. S.; Sen, K., Eds.; *Molecular Electrostatic Potentials, Vol. 3: Concepts and Applications (Theoretical and Computational Chemistry)*; Elsevier Science: 1996. (b) Politzer, P.; Truhlar, D. G. *Chemical Applications of Atomic and Molecular Electrostatic Potentials: Reactivity, Structure, Scattering, and Energetics of Organic, Inorganic, and Biological Systems*; Springer: New York, 1981.
(50) (a) Glaser, R.; Sui, Y.; Sarkar, U.; Gates, K. Electronic Structures and Spin Topologies of γ-Picoliniumyl Radicals. A Study of the Homolysis of *N*-Methyl-γ-Picolinium and of Benzo-, Dibenzo-, and Naphthoannulated Analogs. *J. Phys. Chem. A* **2008**, *112*, 4800−4814. (b) Sui, Y.; Glaser, R.; Sarkar, U.; Gates, K. Stabilities and Spin Density Distributions of Benzannulated Benzyl Radicals. *J. Chem. Theory Comput.* **2007**, *3*, 1091−1099. (c) Glaser, R.; Choy, G. S.-C.; Chen, G. S.; Grützmacher, H. Inductive and Conjugative S→C Polarizations in "Trithiocarbenium Ions" $[C(SH)_3]^+$ and $[C(SH)_3]^{\bullet,2+}$. Potential Energy Surface Analysis, Electronic Structure Motif and Spin Density Distribution. *J. Am. Chem. Soc.* **1996**, *118*, 11617−11628. (d) Glaser, R.; Choy, G. S.-C. Spin Polarization versus Spin Delocalization. Topological Electron and Spin Density Analysis of the Rotational Automerization of Allyl Radical Including Electron Correlation Effects. *J. Phys. Chem.* **1994**, *98*, 11379−11393. (e) Glaser, R.; Choy, G. S.-C. Electron and Spin Density Analysis of Spin-Projected Unrestricted Hartree-Fock Density Matrices of Radicals. *J. Phys. Chem.* **1993**, *97*, 3188−3198.
(51) Frisch, M. J; Trucks, G. W.; Schlegel, H. B.; Scuseria, G. E.; Robb, M. A.; Cheeseman, J. R.; Scalmani, G.; Barone, V.; Mennucci, B.; Petersson, G. A.; Nakatsuji, H.; Caricato, M.; Li, X.; Hratchian, H. P.; Izmaylov, A. F.; Bloino, J.; Zheng, G.; Sonnenberg, J. L.; Hada, M.; Ehara, M.; Toyota, K.; Fukuda, R.; Hasegawa, J.; Ishida, M.; Nakajima, T.; Honda, Y.; Kitao, O.; Nakai, H.; Vreven, T.; Montgomery, J. A., Jr.; Peralta, J. E.; Ogliaro, F.; Bearpark, M.; Heyd, J. J.; Brothers, E.; Kudin, K. N.; Staroverov, V. N.; Keith, T.; Kobayashi, R.; Normand, J.; Raghavachari, K.; Rendell, A.; Burant, J. C.; Iyengar, S. S.; Tomasi, J.; Cossi, M.; Rega, N.; Millam, J. M.; Klene, M.; Knox, J. E.; Cross, J. B.; Bakken, V.; Adamo, C.; Jaramillo, J.; Gomperts, R.; Stratmann, R. E.; Yazyev, O.; Austin, A. J.; Cammi, R.; Pomelli, C.; Ochterski, J. W.; Martin, R. L.; Morokuma, K.; Zakrzewski, V. G.; Voth, G. A.; Salvador, P.; Dannenberg, J. J.; Dapprich, S.; Daniels, A. D.; Farkas, O.; Foresman, J. B.; Ortiz, J. V.; Cioslowski, J.; and Fox, D. J. *Gaussian 09, Revision B.01*; Gaussian, Inc.: Wallingford, CT, 2010.
(52) Miller, S. L.; Aamodt, L. C.; Dousmanis, G.; Townes, C. H.; Kraitchman, J. Structure of Methyl Halides. *J. Chem. Phys.* **1952**, *20*, 1112−1116.
(53) Barss, W. M. *Electron Diffraction in Gases*. Ph.D. Thesis, Purdue University, 1942, p 45ff.
(54) Kornweitz, H.; Raz, T.; Levine, R. D. Driving High Threshold Chemical Reactions by Cluster-Surface Collisions: Molecular Dynamics Simulations for CH_3I Clusters. *J. Phys. Chem. A* **1999**, *103*, 10179−10186.

(55) Maier, G.; Reisenauer, H. P.; De Marco, M. Isomerizations between nitrosyl halides X-N═O and isonitrosyl halides X-O-N: a matrix-spectroscopic study. *Chemistry* **2000**, *6*, 800−808.
(56) Kosmas, A. M.; Drougas, E. The quantum mechanical description of normal valent and multivalent iodine in the polyoxides of the type IO_nX, X=H, CH_3, n = 1, 2, 3. *Comput. Mater. Sci.* **2007**, *38*, 502−505.
(57) Drougas, E; Kosmas, A. M. Ab Initio Characterization of (CH_3IO_3) Isomers and the CH_3O_2 + IO Reaction Pathways. *J. Phys. Chem.* **2007**, *111*, 3402−3408.
(58) (a) Berski, S.; Latajka, Z.; Gordon, A. J. Oxygen bound iodine (O-I): The Electron Localization Function (ELF) study on bonding in cis- and trans-IONO. *Chem. Phys. Lett.* **2011**, *506*, 15−21. (b) Papayannis, D. K.; Kosmas, A. M. Ab initio investigation of isomeric and conformeric structures of halogen nitrites, XONO (X = Cl, Br, I). *Mol. Phys.* **2006**, *104*, 2561−2567.
(59) Papayannis, D. K.; Kosmas, A. M. Theoretical investigation of the mechanism of the reaction IO + NO → I + NO_2. *Chem. Phys. Lett.* **2006**, *432*, 391−397.
(60) The nomenclature reflects that **5** is the most stable aggregate on the potential energy surface (PES).
(61) Griller, D.; Kanabus-Kaminskaa, J. M.; Maccoll, A. Bond Dissociation Energies For Common Organic Compounds. *J. Mol. Struct.* **1988**, *163*, 125−131.
(62) Carson, A. S.; Carter, W.; Pedley, J. B. The thermochemistry of reductions caused by lithium aluminum hydride. I. The C−I bond dissociation energy in CH_3I. *Proc. R. Soc. London, Ser. A* **1961**, *260*, 550−557.
(63) Zhang, J.-X.; Li, Z.-S.; Liu, J.-Y.; Sun, C.-C. Theoretical mechanistic study on the radical-molecule reaction of $CHCl_2/CCl_3$ with NO_2. *J. Comput. Chem.* **2006**, *27*, 661−671.
(64) Cole, S. K.; Cooper, W. J.; Fox, R. V.; Gardinali, P. R.; Mezyk, S. P.; Mincher, B. J.; O'Shea, K. E. Free Radical Chemistry of Disinfection Byproducts. 2. Rate Constants and Degradation Mechanisms of Trichloronitromethane (Chloropicrin). *Environ. Sci. Technol.* **2007**, *41*, 863−869.